

## Topological pathways to two-dimensional quantum turbulence

R. Panico<sup>1,2</sup>, G. Ciliberto<sup>3</sup>, G. I. Martone<sup>1,4</sup>, T. Congy<sup>5</sup>, D. Ballarini<sup>1</sup>, A. S. Lanotte<sup>1,4</sup> and N. Pavloff<sup>3,6</sup>

<sup>1</sup>*CNR NANOTEC, Institute of Nanotechnology, Via Monteroni, 73100 Lecce, Italy*

<sup>2</sup>*Institut für Angewandte Physik, Universität Bonn, Wegelerstraße 8, 53115 Bonn, Germany*

<sup>3</sup>*Université Paris-Saclay, CNRS, LPTMS, 91405 Orsay, France*

<sup>4</sup>*INFN, Sezione di Lecce, 73100 Lecce, Italy*

<sup>5</sup>*Department of Mathematics, Physics and Electrical Engineering, Northumbria University, Newcastle upon Tyne NE1 8ST, United Kingdom*

<sup>6</sup>*Institut Universitaire de France (IUF)*



(Received 11 November 2024; revised 11 February 2025; accepted 8 April 2025; published 11 June 2025; corrected 16 June 2025)

We present a combined experimental and theoretical investigation of the formation and decay kinetics of vortices in two-dimensional, compressible quantum turbulence. We follow the temporal evolution of a quantum fluid of exciton polaritons, hybrid light-matter quasiparticles, and measure both phase and modulus of the order parameter in the turbulent regime. Fundamental topological conservation laws require that the formation and annihilation of vortices also involve critical points of the velocity field, namely nodes and saddles. Identifying the simplest mechanisms underlying these processes enables us to develop an effective kinetic model that closely aligns with the experimental observations, and shows that different processes are responsible for vortex number growth and decay. These findings underscore the crucial role played by topological constraints in shaping nonlinear, turbulent evolution of two-dimensional quantum fluids.

DOI: [10.1103/PhysRevResearch.7.L022063](https://doi.org/10.1103/PhysRevResearch.7.L022063)

**Introduction.** Topological and dynamical properties of two-dimensional systems are strongly intertwined. This is true not only in condensed matter setups [1–3] but also for hydrodynamical systems, be these classical or quantum. In classical fluids the identification of topological critical points proves helpful for classifying flow patterns [4,5] and studying two-dimensional spatiotemporal chaos and turbulence [6–10]. As for quantum fluids, the importance of quantization of vorticity has been understood long ago [11,12] and vortices indeed play a major role in the route to two-dimensional quantum turbulence [13–22], as they do in the classical context [23–27]. In this Letter, we further explore the link between dynamical and topological properties in two-dimensional quantum turbulence. We propose to investigate the temporal properties of the quantum fluid velocity field by a novel strategy. The idea is to devise a minimal model, which complies with global topological constraints, without requiring local knowledge of the spatial dynamics of the system. To achieve this, we derive kinetic equations of formation and annihilation of critical points of the velocity field, and apply the approach to a nonequilibrium exciton-polariton fluid. We show that we can reproduce the experimentally observed rate of creation and annihilation of quantized vortices, thus identifying the elementary mechanisms responsible for the increase in the number of vortices, during the quantum turbulence

growth, and for its reduction, during the quantum turbulence decay.

We consider a two-dimensional quantum fluid described by a scalar order parameter of the form  $\psi(\vec{r}, t) = A(\vec{r}, t) \exp[i\Theta(\vec{r}, t)]$ . Here the real functions  $A (\geq 0)$  and  $\Theta$  correspond to the amplitude and phase of the order parameter, respectively, and  $\vec{r} = (x, y)$ . The velocity field of the fluid is  $\vec{v} = (\hbar/m)\vec{\nabla}\Theta$  [12]. In a two-dimensional setting, two topological indices are associated with any domain  $D$  delimited by a close contour  $C$ , namely, the vorticity  $I_V$  and the Poincaré index  $I_P$  [28]

$$I_V = \frac{1}{2\pi} \oint_C d\Theta, \quad I_P = \frac{1}{2\pi} \oint_C d\varphi, \quad (1)$$

where  $\varphi$  denotes the polar angle of  $\vec{v}$ .

$I_V$  is (up to a factor  $2\pi$ ) the variation of the phase  $\Theta$  along the contour  $C$ .  $I_P$  is the net algebraic number of revolutions made by the velocity field's direction along  $C$  [29]. It is interesting to note that what is commonly referred to as the vorticity in the context of the two-dimensional  $xy$  model is actually the Poincaré index; see, e.g., Refs. [30,31]. Both indices are zero if there are no singular nor stagnation points inside  $D$ . They assume nontrivial values when the phase  $\Theta$  displays extrema (local maxima or minima), saddles, or essential singularities. The corresponding points are nodes (attractive or repulsive), saddles, and quantum vortices, respectively. Figure 1 gives the values of the indices attached to each of these points, which we loosely denote as critical points in the following. The vorticity and Poincaré index attached to a given domain are the sum of the indices of all the critical points it contains.

Published by the American Physical Society under the terms of the [Creative Commons Attribution 4.0 International](https://creativecommons.org/licenses/by/4.0/) license. Further distribution of this work must maintain attribution to the author(s) and the published article's title, journal citation, and DOI.

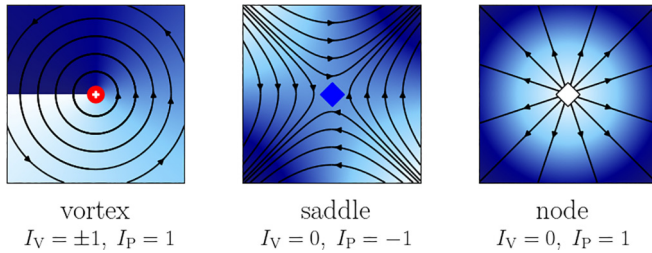


FIG. 1. Sketch of the streamline pattern around a (positive) vortex, a saddle, and a node (phase minimum). Darker regions correspond to larger values of the phase  $\Theta$  of the order parameter. A vortex is a branch point of the phase, the corresponding branch cut is represented by a discontinuity of the color map in the left plot. Nodes and saddles are stagnation points where  $\vec{v} = \vec{0}$ .

The coexistence of the three types of critical points presented in Fig. 1 has been explicitly experimentally demonstrated in linear [32] and nonlinear [33] optics. The physical system we examine here involves injecting a high-energy polariton superfluid, and allowing it to expand within a circular potential barrier [22]. The initial kinetic energy provided to the superfluid induces the creation not only of a dense vortex gas but also of a large number of saddles and nodes. The optical nature of polaritons allows for the measurement of both the modulus and the phase of the order parameter through interferometric techniques [21,34,35], which enables recording the flow pattern with a level of detail currently unattainable in other types of superfluids. As shown in Fig. 2, by analyzing the velocity field, we can track the evolution of hundreds of critical points. This method enables us to determine, at each time step, the number of vortices, saddles, and nodes present in the system. We emphasize that the presence of nodes is a unique feature of compressible and nonstationary quantum fluids, such as polariton superfluids. These nodes are indeed observed in our experimental results, and we demonstrate below that they play a crucial role in the onset of turbulence.

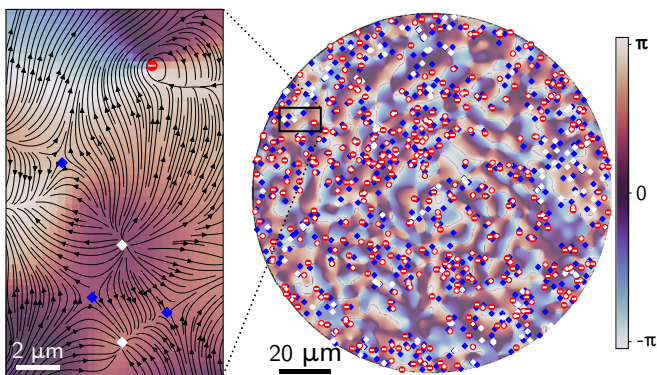
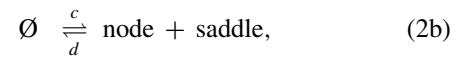
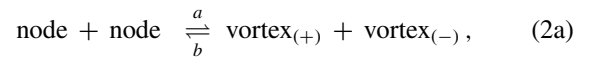


FIG. 2. A snapshot of the polariton superfluid phase field, with the measured critical points. The three types of critical points are represented with the same symbols as in Fig. 1. A zoom, with streamlines represented as oriented solid lines, highlights the local flow organization, revealing three saddles, two nodes (one attractive and one repulsive), and a negative vortex.

*Model.* We consider the following main mechanisms of creation (or annihilation) of critical points in the flow field: (i) the nodes-to-vortices conversion in which two nodes coalesce and give birth to two vortices and (ii) the saddle-node bifurcation, which creates one saddle and one node from scratch. These two processes conserve the vorticity and the Poincaré index; they correspond to well-identified bifurcations whose relevance for a two-dimensional quantum fluid has been validated in Ref. [33]. They can be schematically written as chemical reactions:



where vortices with positive or negative vorticity are denoted as  $\text{vortex}_{(+)}$  or  $\text{vortex}_{(-)}$ , respectively. The (positive) quantities  $a$ ,  $b$ ,  $c$ , and  $d$  are the reaction rates, see Eq. (3) below. Mechanism (2a) appeared implicitly in works by Indebetouw [36] and the Soskin group [37], then explicitly in Ref. [38]. Mechanism (2b) is mentioned by Freund in Ref. [39]. Other mechanisms have been observed [33], which also conserve both the vorticity and the Poincaré index: a saddle can transform into two saddles plus one node in a pitchfork bifurcation, or also a vortex-antivortex pair and two saddles can appear spontaneously (or coalesce) in a process first identified by Nye *et al.*, [28], which has been termed the “Bristol mechanism” in Ref. [33]. These reactions have been discarded for simplicity reasons (they involve collisions of a larger number of critical points) and also because much less often observed in a previous experiment and in numerical simulations [33].

From the modeling (2), we write a kinetic equation inspired by rate equations of elementary chemical reactions:

$$\begin{aligned} \frac{dV_{\pm}}{dt} &= aN^2 - bV_+V_-, & \frac{dS}{dt} &= c - dNS, \\ \frac{dN}{dt} &= -2aN^2 + 2bV_+V_- + c - dNS, \end{aligned} \quad (3)$$

where  $N(t)$  denotes the number of nodes,  $S(t)$  the number of saddles, and  $V_+(t)$  [ $V_-(t)$ ] the number of vortices with positive [negative] vorticity. It results from the values of the topological indices listed in Fig. 1 that the total Poincaré index of the system is  $I_p = N + V_+ + V_- - S$ . It is easily verified that  $I_p$  is preserved by the system (3): this comes as no surprise since the elementary processes (2) both conserve the Poincaré index. Similarly, the conserved total vorticity of the system is  $V_+ - V_-$ . In the following we make the simplifying assumption that this difference is equal to zero:  $V_+(t) = V_-(t) = V(t)/2$  where  $V(t)$  is the total number of vortices. This hypothesis is confirmed by the experimental data (such as displayed in Fig. 3) and is certainly sound in the configuration we consider where typically  $V(t) \gg 1$  while no external angular momentum is imparted to the system.

Defining the rescaled quantities  $\tau = t/t_0$ ,  $n = N/N_0$ ,  $v = V/N_0$ , and  $s = S/N_0$ , with  $t_0 = 1/\sqrt{2ac}$  and  $N_0 = \sqrt{c/2a}$ , makes it possible to cast the system (3) under the following

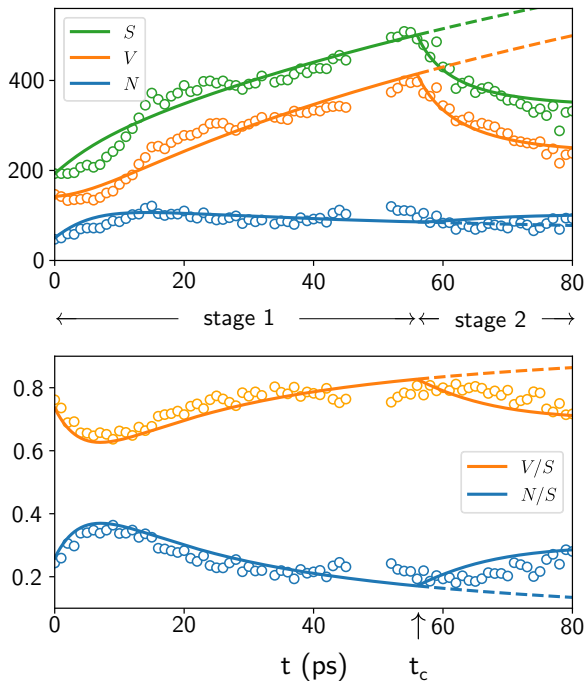


FIG. 3. (Top) Comparison of the experimental results for  $N(t)$ ,  $V(t)$  and  $S(t)$  (circles) with the theoretical predictions (lines). Experimental data are averages of four realizations of the same dynamical regime. For  $t \leq t_c$ , the solid lines have been obtained with the numerical integration of Eqs. (4) with the values  $\gamma = 0.52$ ,  $N_0 = 170$ , and  $t_0 = 11$  ps [40]. For  $t > t_c$ , the dashed lines correspond to the results of (4), while the solid lines come from the numerical resolution of (6) with  $\varepsilon = 0.045$ . (Bottom) Same as above for the quantities  $V(t)/S(t)$  and  $N(t)/S(t)$ . The value of  $t_c$  is 56 ps.

dimensionless form:

$$\begin{aligned} \frac{dv}{d\tau} &= n^2 - \alpha v^2, & \frac{ds}{d\tau} &= 1 - \gamma ns, \\ \frac{dn}{d\tau} &= 1 - n^2 - \gamma ns + \alpha v^2, \end{aligned} \quad (4)$$

where  $\alpha = b/(4a)$  and  $\gamma = d/(2a)$  [41].

**Results.** We consider a turbulent regime of the polariton dynamics in which, after fast expansion of the quantum fluid, the onset of vortex clustering and the emergence of the inverse kinetic energy cascade was evidenced on timescales of a few tens of picoseconds [22]. The numbers of vortices, saddles and nodes, extracted from the data of Ref. [22], are displayed as circles in the top part of Fig. 3. At  $t = 0$ , when the fluid hits the barrier, some critical points are already present, having formed during the fluid's expansion. The turbulent dynamics is initiated at this moment, which we treat as the initial condition. A low-energy data set, where the onset of turbulence is inhibited by dissipation, is presented in Ref. [42] along with additional details on the experimental configuration. Let us first focus on the stage of turbulence growth, during which the numbers of vortices and saddles increase significantly (stage 1 in Fig. 3). In this time lag, the nucleation of many new vortices and saddles dominates the temporal evolution. This implies imposing  $\alpha = 0$ : indeed, when  $\alpha \neq 0$  the system (4) has a fixed point and the numbers of vortices, saddles,

and nodes tend to saturate, which is not what is observed in the experiment. We checked that a nonzero value of  $\alpha$  always worsens the agreement of the theoretical curve with data: this confirms that in this stage the incompressible kinetic energy of the system is mostly increasing, as required for the establishment of the inverse cascade of kinetic energy, see the Discussion section below.

It is interesting to discuss the values of the rate of reactions in Eqs. (2). In particular  $c/d = N_0^2/\gamma = 6 \times 10^4 \gg 1$ , implying that the saddle-node bifurcation is mainly unidirectional: the annihilation of a saddle with a node is much less frequent than their *creatio ex nihilo*. This indicates that the saddle-node formation mechanism (2b) is the real fuel of the whole process. The nodes-to-vortices reaction (2a) merely transmutes some of the nodes into vortices, but could not be effective on its own. This remark is of significance: the spontaneous creation of uniquely a vortex-antivortex pair being topologically forbidden (it would not conserve the Poincaré index) we are in need of an explanation of the increase of the number  $V(t)$  of vortices. In the system we consider, the formation of vortices arises from two saddle-nodes bifurcations (2a) followed by a nodes-to-vortices conversion (2b), ultimately resulting in the formation of two saddles and two vortices. This is the reason why, as shown in the top part of Fig. 3, the numbers of saddles and of vortices increase at the same pace. The results plotted in the bottom panel of Fig. 3 indicate that the total Poincaré index is conserved and small. Indeed in this case  $N + V = S$ , the two quantities  $V/S$  and  $N/S$  sum to unity, and a minimum of one should correspond to a maximum of the other. This property is model independent: it is a prerequisite, which should be embodied in any kinetic model, but its fulfillment is not a guarantee of accuracy of the model. Experimental results confirm the exact conservation of both  $I_V$  and  $I_P$  indices in every realization of the measurements.

The results displayed in Fig. 3 show a striking behavior, namely, a sharp temporal transition from stage 1, characterized by the nonlinear growth of the number of vortices and saddles, to stage 2, characterized by a dramatic decrease of the number of vortices and saddles. However, the number of nodes is not experiencing a similar abrupt modification in the same period of time: this supports a scenario, which does not involve nodes, still conserving both  $I_V$  and  $I_P$ . The so-called Bristol mechanism [28], described by Eq. (5) below, is a perfect candidate:



In view of the significant decrease of the number of vortices and saddles during stage 2, we consider that the rate of reaction  $f$  is zero in Eq. (5). Hence, the process is assumed to be unidirectional [43]. The system (4) accordingly modifies to

$$\begin{aligned} \frac{dv}{d\tau} &= n^2 - \alpha v^2 - \varepsilon v^2 s^2, & \frac{ds}{d\tau} &= 1 - \gamma ns - \varepsilon v^2 s^2, \\ \frac{dn}{d\tau} &= 1 - n^2 - \gamma ns + \alpha v^2, \end{aligned} \quad (6)$$

where  $\varepsilon = \frac{1}{2}eN_0^3t_0 = ec/(8a^2)$  is the rescaled rate of annihilation of saddles and vortices. We keep for all the other parameters the values previously determined, and during stage 2 we solve the system (6) with  $\varepsilon \neq 0$ . The corresponding

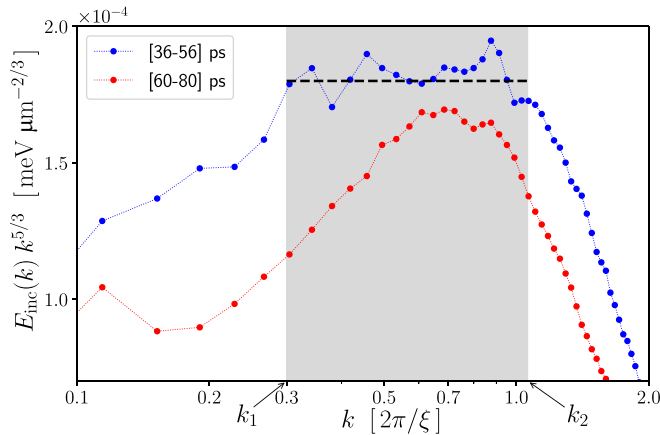


FIG. 4. Compensated experimental spectra of the incompressible kinetic energy, averaged over two different time windows: during the stage in which the inverse cascade develops ([36–56] ps), and during the decay stage ([60–80] ps). The gray area identifies the spectral region of wave numbers, the so-called inertial range, associated to the inverse cascade of the incompressible kinetic energy  $k_1 < k < k_2$ , where  $k_1 \xi / 2\pi = 0.3$  and  $k_2 \xi / 2\pi = 1.06$ ,  $\xi = \hbar(2mg|\psi|^2)^{-1/2}$  being the healing length. The horizontal dashed line is just a guide for the eye.

results are displayed in Fig. 3. The agreement of the theoretical curve with the experimental observation supports the idea that after  $t = t_c$  the system enters a new regime in which the annihilation mechanism (5) acquires an efficiency it previously did not have.

It is interesting to ask the question whether the mechanism of Eq. (5), which is explicitly observed in our experiment [42], could have been effective earlier, with a rate of reaction  $f \neq 0$  explaining the rapid and concomitant increase of  $V$  and  $S$  during stage 1. The observation of the behavior of  $N$  in the same period makes this hypothesis rather unlikely, since  $N$  initially increases and then saturates. This advocates for a saddle-node creation process (2b), which then feeds the nodes-to-vortices one (2a). Only this process can explain (i) the occurrence of extrema of  $V/S$  and  $N/S$  at short times (bottom plot of Fig. 3) and (ii) the saturation of  $N$  at a slightly later time (top plot of the same figure). And indeed, it is not possible to accurately reproduce the experimental data on the basis of mechanisms (2a) and (5) only, or (2b) and (5) only.

*Discussion.* The sharp modification of the time evolution of the number of vortices and saddles at  $t_c = 56$  ps is well described by the inclusion of the Bristol mechanism (5), but the very fact that such a transition occurs is not explained by our model. We show here that this transition occurs exactly at the time where the inverse turbulent cascade stops.

In Fig. 4 we reanalyze the data of Ref. [22] by displaying the experimental one-dimensional spectra of the incompressible kinetic energy  $E_{\text{inc}}(k)$ , where  $k = |\vec{k}|$  [44], averaged over two different time windows. In the gray area for wave numbers  $k_1 < k < k_2$ , the average of spectra measured for time lags  $t \in [36, 56]$  ps (blue points in Fig. 4) exhibits a behavior compatible with the expected Kolmogorov-like scaling [45],  $E_{\text{inc}}(k) \propto k^{-5/3}$  [46]. This tendency no longer persists beyond  $t_c$ : the average of spectra measured for  $t \in [60, 80]$  ps (red points in Fig. 4) displays a narrower scaling region and a

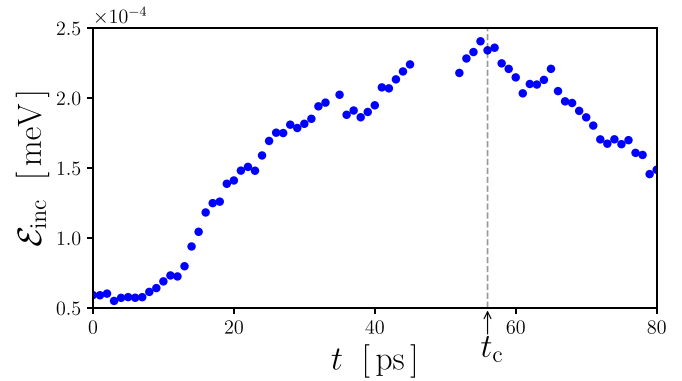


FIG. 5. Time evolution of the incompressible kinetic energy  $\mathcal{E}_{\text{inc}}(t)$  defined in Eq. (7).

smaller amplitude. These are both indications of the end of the inverse cascade.

This trend is further confirmed by an analysis of the temporal behavior of the part of the incompressible kinetic energy contained within the inertial range of the inverse cascade (i.e., for  $k \in [k_1, k_2]$ ), that we call  $\mathcal{E}_{\text{inc}}(t)$ . This quantity is defined by

$$\mathcal{E}_{\text{inc}}(t) \equiv \int_{k_1}^{k_2} E_{\text{inc}}(k, t) dk. \quad (7)$$

Its evaluation is made possible by the recording at each time lag of the experimental spectrum  $E_{\text{inc}}(k, t)$ .  $\mathcal{E}_{\text{inc}}(t)$ , plotted in Fig. 5, is an estimate of the energy available to establish the inverse cascade process. The onset of a turbulent inverse cascade of kinetic energy implies a temporal growth of the incompressible part of the total kinetic energy in the system. Indeed, the results show that, after setup time,  $\mathcal{E}_{\text{inc}}(t)$  goes on growing as expected, until the critical time  $t_c = 56$  ps. At this stage the available incompressible kinetic energy starts its decay and can no longer sustain the inverse transfer process across scales.

The fact that the crossover time  $t_c$  is observed during the growth then simultaneous rapid decrease of both the vortices and saddles numbers, and that  $t_c$  also marks the end of the temporal growth of the incompressible kinetic energy, suggests that these processes are fed by the incompressible kinetic energy available in the inertial range. When this stops growing, dissipation mechanisms prevail and turbulence starts decaying. Interestingly, at the same time the clustering dynamics stops [42].

*Conclusion.* In the experiments we presented, dynamical observations associated to the turbulence growth/decay have their topological counterpart in the time window where the numbers of vortices and saddles increase/decrease. It is reasonable to think that not all vortices participate in the cascade, since they may not have time to correlate, nevertheless their increase reflects in the growth of the incompressible kinetic energy available for the cascade.

Topological constraints also rule the mechanism of the turbulence decay; a process based on four-vortex interactions [47] previously proposed in Refs. [48–52], here finds its origin in topological arguments. In the absence of a turbulent regime, the fate of vortices is different. In such a case, we physically expect a dynamical equilibrium between vortex creation and

annihilation processes, in the presence of random, uncorrelated fluctuations. Our model faithfully describe this process, see Ref. [42].

The kinetic model here introduced is the simplest that complies with topological constraints. It provides a global, averaged description of the system based on phenomenological parameters (the rate coefficients) but is not designed to explain why these parameters assume different values in the turbulent or non-turbulent regimes, nor to predict when turbulence growth halts and why its decay is so abrupt. Addressing these phenomena requires to account for vortex clustering, i.e., to deal with spatial correlations within the system.

This focus on spatial correlations is crucial in the study of two-dimensional turbulence: since Polyakovs pioneering contribution [53] it has been shown that the vorticity domains exhibit the same universal scaling arising in critical percolation theory, in both classical [54,55] and quantum [56] fluids in the regime of inverse energy cascade. Broadening the scope of our kinetic approach to set up a microscopic model that integrates these statistical properties would therefore be of great interest. Such a model should account for interactions between critical points (such as vortex clustering) within a framework consistent with the conservation of topological indices.

*Acknowledgments.* N.P. acknowledges insightful comments by M. V. Berry and M. R. Dennis. D.B., T.C., and A.S.L. acknowledge the kind hospitality during the workshop

“Turbulence and Vortex dynamics in 2D quantum fluids” at the International Center for Theoretical Sciences (ICTS, Bangalore, India), (code: ICTS/QUFLU2024/2). T.C. and N.P. thank the Isaac Newton Institute for Mathematical Sciences, Cambridge, for support and hospitality during the programme Emergent Phenomena in Nonlinear Dispersive Waves, where the work on this paper was partially undertaken. This work was supported by the Italian Ministry of University and Research (MUR) through the PNRR MUR project: ‘National Quantum Science and Technology Institute’ - NQSTI (PE0000023) and the PNRR MUR project: ‘Integrated Infrastructure Initiative in Photonic and Quantum Sciences’ - I-PHOQSI (IR00000163). We acknowledge the support of the Quantum Optical Networks based on Exciton-polaritons - (Q-ONE) funding from the HORIZON-EIC-2022-PATHFINDER CHALLENGES EU programme under Grant Agreement No. 101115575, and of the Neuro-morphic Polariton Accelerator - (PolArt) funding from the Horizon-EIC-2023-Pathfinder Open EU programme under Grant Agreement No. 101130304. Views and opinions expressed are, however, those of the author(s) only and do not necessarily reflect those of the European Union or European Innovation Council and SMEs Executive Agency (EISMEA). Neither the European Union nor the granting authority can be held responsible for them.

*Data availability.* The data that support the findings of this article are available upon reasonable request from the authors.

- 
- [1] X.-L. Qi and S.-C. Zhang, Topological insulators and superconductors, *Rev. Mod. Phys.* **83**, 1057 (2011).
- [2] D. Culcer, A. C. Keser, Y. Li, and G. Tkachov, Transport in two-dimensional topological materials: recent developments in experiment and theory, *2D Mater.* **7**, 022007 (2020).
- [3] C. Reichhardt, C. J. O. Reichhardt, and M. V. Milošević, Statics and dynamics of skyrmions interacting with disorder and nanostructures, *Rev. Mod. Phys.* **94**, 035005 (2022).
- [4] M. J. Lighthill, Introduction. boundary layer theory, in *Laminar Boundary Layer*, edited by L. Rosenhead (Dover Publications, New York, 1966), Chap. II, p. 46.
- [5] A. Perry and B. Fairlie, Critical points in flow patterns, in *Turbulent Diffusion in Environmental Pollution*, Advances in Geophysics Vol. 18B, edited by F. Frenkiel and R. Munn (Elsevier, Amsterdam, 1975), pp. 299–315.
- [6] H. K. Moffatt, The topology of scalar fields in 2D and 3D turbulence, in *IUTAM Symposium on Geometry and Statistics of Turbulence*, edited by T. Kambe, T. Nakano, and T. Miyauchi (Springer Netherlands, Dordrecht, 2001), pp. 13–22.
- [7] L. Rossi, J. C. Vassilicos, and Y. Hardalupas, Multiscale laminar flows with turbulentlike properties, *Phys. Rev. Lett.* **97**, 144501 (2006).
- [8] N. T. Ouellette and J. P. Gollub, Dynamic topology in spatiotemporal chaos, *Phys. Fluids* **20**, 064104 (2008).
- [9] J. M. Garcia de la Cruz, J. C. Vassilicos, and L. Rossi, Topologies of velocity-field stagnation points generated by a single pair of magnets in free-surface electromagnetic experiments, *Phys. Rev. E* **90**, 043001 (2014).
- [10] S. S. Smith, J. Arenson, E. Roberts, S. Sindi, and K. A. Mitchell, Topological chaos in a three-dimensional spherical fluid vortex, *Europhys. Lett.* **117**, 60005 (2017).
- [11] L. Onsager, Statistical hydrodynamics, *Nuovo Cim.* **6**, 279 (1949).
- [12] R. P. Feynman, Application of quantum mechanics to liquid helium, in *Progress in Low Temperature Physics*, edited by C. J. Gorter (Elsevier, New York, 1955), Vol. 1, Chap. II, pp. 17–53.
- [13] S. Nazarenko and M. Onorato, Wave turbulence and vortices in Bose–Einstein condensation, *Physica D* **219**, 1 (2006).
- [14] T. W. Neely, A. S. Bradley, E. C. Samson, S. J. Rooney, E. M. Wright, K. J. H. Law, R. Carretero-González, P. G. Kevrekidis, M. J. Davis, and B. P. Anderson, Characteristics of two-dimensional quantum turbulence in a compressible superfluid, *Phys. Rev. Lett.* **111**, 235301 (2013).
- [15] A. C. White, B. P. Anderson, and V. S. Bagnato, Vortices and turbulence in trapped atomic condensates, *Proc. Natl. Acad. Sci. USA* **111**, 4719 (2014).
- [16] Y. P. Sachkou, C. G. Baker, G. I. Harris, O. R. Stockdale, S. Forstner, M. T. Reeves, X. He, D. L. McAuslan, A. S. Bradley, M. J. Davis, and W. P. Bowen, Coherent vortex dynamics in a strongly interacting superfluid on a silicon chip, *Science* **366**, 1480 (2019).
- [17] G. Gauthier, M. T. Reeves, X. Yu, A. S. Bradley, M. A. Baker, T. A. Bell, H. Rubinsztein-Dunlop, M. J. Davis, and T. W. Neely, Giant vortex clusters in a two-dimensional quantum fluid, *Science* **364**, 1264 (2019).

- [18] S. P. Johnstone, A. J. Groszek, P. T. Starkey, C. J. Billington, T. P. Simula, and K. Helmerson, Evolution of large-scale flow from turbulence in a two-dimensional superfluid, *Science* **364**, 1267 (2019).
- [19] A. Forrester, H.-C. Chu, and G. A. Williams, Renormalized analytic solution for the enstrophy cascade in two-dimensional quantum turbulence, *Phys. Rev. Fluids* **5**, 072701(R) (2020).
- [20] A. Eloy, O. Boughdad, M. Albert, P.-É. Larré, F. Mortessagne, M. Bellec, and C. Michel, Experimental observation of turbulent coherent structures in a superfluid of light, *Europhys. Lett.* **134**, 26001 (2021).
- [21] M. Baker-Rasooli, W. Liu, T. Aladjidi, A. Bramati, and Q. Glorieux, Turbulent dynamics in a two-dimensional paraxial fluid of light, *Phys. Rev. A* **108**, 063512 (2023).
- [22] R. Panico, P. Comaron, M. Matuszewski, A. S. Lanotte, D. Trypogeorgos, G. Gigli, M. De Giorgi, V. Ardizzone, D. Sanvitto, and D. Ballarini, Onset of vortex clustering and inverse energy cascade in dissipative quantum fluids, *Nat. Photon.* **17**, 451 (2023).
- [23] J. C. McWilliams, The emergence of isolated coherent vortices in turbulent flow, *J. Fluid Mech.* **146**, 21 (1984).
- [24] A. Babiano, C. Basdevant, B. Legras, and R. Sadourny, Vorticity and passive-scalar dynamics in two-dimensional turbulence, *J. Fluid Mech.* **183**, 379 (1987).
- [25] R. Benzi, S. Patarnello, and P. Santangelo, On the statistical properties of two-dimensional decaying turbulence, *Europhys. Lett.* **3**, 811 (1987).
- [26] M. E. Brachet, M. Meneguzzi, H. Politano, and P. L. Sulem, The dynamics of freely decaying two-dimensional turbulence, *J. Fluid Mech.* **194**, 333 (1988).
- [27] G. Boffetta and R. E. Ecke, Two-dimensional turbulence, *Annu. Rev. Fluid Mech.* **44**, 427 (2012).
- [28] J. F. Nye, J. V. Hajnal, and J. H. Hannay, Phase saddles and dislocations in two-dimensional waves such as the tides, *Proc. R. Soc. Lond. A* **417**, 7 (1988).
- [29] S. H. Strogatz, *Nonlinear Dynamics and Chaos: With Applications to Physics, Biology, Chemistry, and Engineering*, 2nd ed. (Westview Press, Boulder, 2015).
- [30] J. M. Kosterlitz and D. J. Thouless, Ordering, metastability and phase transitions in two-dimensional systems, *J. Phys. C* **6**, 1181 (1973).
- [31] J. M. Kosterlitz, The critical properties of the two-dimensional xy model, *J. Phys. C* **7**, 1046 (1974).
- [32] N. Shvartsman and I. Freund, Speckle spots ride phase saddles sidesaddle, *Opt. Commun.* **117**, 228 (1995).
- [33] T. Congy, P. Azam, R. Kaiser, and N. Pavloff, Topological constraints on the dynamics of vortex formation in a two-dimensional quantum fluid, *Phys. Rev. Lett.* **132**, 033804 (2024).
- [34] D. Caputo, N. Bobrovska, D. Ballarini, M. Matuszewski, M. De Giorgi, L. Dominici, K. West, L. N. Pfeiffer, G. Gigli, and D. Sanvitto, Josephson vortices induced by phase twisting a polariton superfluid, *Nat. Photon.* **13**, 488 (2019).
- [35] K. A. Sitnik, S. Alyatkin, J. D. Töpfer, I. Gnusov, T. Cookson, H. Sigurdsson, and P. G. Lagoudakis, Spontaneous formation of time-periodic vortex cluster in nonlinear fluids of light, *Phys. Rev. Lett.* **128**, 237402 (2022).
- [36] G. Indebetouw, Optical vortices and their propagation, *J. Mod. Opt.* **40**, 73 (1993).
- [37] M. S. Soskin, V. N. Gorshkov, M. V. Vasnetsov, J. T. Malos, and N. R. Heckenberg, Topological charge and angular momentum of light beams carrying optical vortices, *Phys. Rev. A* **56**, 4064 (1997).
- [38] M. S. Soskin, V. N. Gorshkov, and M. V. Vasnetsov, Topology of light: wave-front and structure of phase vortices, extrema, and saddles, *Ukr. J. Phys.* **44**, 24 (1999).
- [39] I. Freund, “1001” correlations in random wave fields, *Waves Random Media* **8**, 119 (1998).
- [40] The quality of the agreement does not sensibly depend on the values of the parameters  $\gamma$ ,  $N_0$ , and  $t_0$ . Numerical checks indicate that the values of these fitting parameters are fixed with a relative uncertainty of the order of 10%.
- [41] For completeness, note that in terms of the new parameters, the rates of reaction read  $a = 1/2N_0t_0$ ,  $b = 2\alpha/N_0t_0$ ,  $c = N_0/t_0$ , and  $d = \gamma/N_0t_0$ .
- [42] See Supplemental Material at <http://link.aps.org/supplemental/10.1103/PhysRevResearch.7.L022063> for the experimental method, instances of direct observation of the Bristol and nodes-to-vortices mechanisms, discusses vortex clustering, presents results for a low injection energy, nonturbulent flow, which includes Ref. [57].
- [43] This unidirectional behavior was already observed in the experiment and the numerical simulations of Ref. [33]: In this reference the Bristol mechanism was always inducing the concomitant annihilation of two vortices and two saddles, and never their *creatio ex nihilo*.
- [44] The density-weighted superfluid velocity field  $\vec{u}(\vec{r}, t) = |\psi|\vec{v}$ , where  $|\psi|^2$  is the number density of the polaritons, is separated into two components: a divergence-free one ( $\vec{u}_{\text{inc}}$ ), which is the incompressible part, and an irrotational one ( $\vec{u}_{\text{comp}}$ ), which is the compressible part. The one-dimensional spectral density of the incompressible kinetic energy is obtained by integrating over the polar angle:  $E_{\text{inc}}(k, t) = \frac{1}{2}mk \int d\theta_k |\vec{u}_{\text{inc}}(\vec{k}, t)|^2$ , see Ref. [58] and the supplementary information of Ref. [22].
- [45] R. H. Kraichnan, Inertial ranges in two-dimensional turbulence, *Phys. Fluids* **10**, 1417 (1967).
- [46] A Kolmogorov-like scaling for the inverse energy cascade in compressible flows has been reported for classical fluids in Ref. [55]. Its experimental realisation in compressible quantum flows [22] is a nontrivial observation by itself.
- [47] Note that since in the observed dynamics, saddles and vortices have similar temporal evolutions, the decay due to the Bristol mechanism (5) is effectively equivalent to a four-vortex decay process.
- [48] S. Nazarenko and M. Onorato, Freely decaying turbulence and Bose–Einstein condensation in Gross–Pitaevski model, *J. Low Temp. Phys.* **146**, 31 (2007).
- [49] A. J. Groszek, T. P. Simula, D. M. Paganin, and K. Helmerson, Onsager vortex formation in Bose–Einstein condensates in two-dimensional power-law traps, *Phys. Rev. A* **93**, 043614 (2016).
- [50] M. Karl and T. Gasenzer, Strongly anomalous non-thermal fixed point in a quenched two-dimensional Bose gas, *New J. Phys.* **19**, 093014 (2017).
- [51] A. W. Baggaley and C. F. Barenghi, Decay of homogeneous two-dimensional quantum turbulence, *Phys. Rev. A* **97**, 033601 (2018).
- [52] T. Kanai and C. Zhang, Dynamical transition of quantum vortex-pair annihilation in a Bose–Einstein condensate [arXiv:2407.14627](https://arxiv.org/abs/2407.14627).

- [53] A. M. Polyakov, The theory of turbulence in two dimensions, *Nucl. Phys. B* **396**, 367 (1993).
- [54] D. Bernard, G. Boffetta, A. Celani, and G. Falkovich, Conformal invariance in two-dimensional turbulence, *Nat. Phys.* **2**, 124 (2006).
- [55] L. Puggioni, A. G. Kritsuk, S. Musacchio, and G. Boffetta, Conformal invariance of weakly compressible two-dimensional turbulence, *Phys. Rev. E* **102**, 023107 (2020).
- [56] R. Panico, A. S. Lanotte, D. Trypogeorgos, G. Gigli, M. De Giorgi, D. Sanvitto, and D. Ballarini, Conformal invariance of 2D quantum turbulence in an exciton–polariton fluid of light, *Appl. Phys. Rev.* **10**, 041418 (2023).
- [57] A. C. White, C. F. Barenghi, and N. P. Proukakis, Creation and characterization of vortex clusters in atomic Bose-Einstein condensates, *Phys. Rev. A* **86**, 013635 (2012).
- [58] C. Nore, M. Abid, and M. E. Brachet, Kolmogorov turbulence in low-temperature superflows, *Phys. Rev. Lett.* **78**, 3896 (1997).
- Correction:* The Editors’ Suggestion label was missing at publication and has been added.

# Supplemental material to: Topological Pathways to Two-Dimensional Quantum Turbulence

R. Panico,<sup>1,2</sup> G. Ciliberto,<sup>3</sup> G. I. Martone,<sup>1,4</sup> T. Congy,<sup>5</sup> D. Ballarini,<sup>1</sup> A. S. Lanotte,<sup>1,4</sup> and N. Pavloff<sup>3,6</sup>

<sup>1</sup>*CNR NANOTEC, Institute of Nanotechnology, Via Monteroni, 73100 Lecce, Italy*

<sup>2</sup>*Institut für Angewandte Physik, Universität Bonn, Wegelerstraße 8, 53115 Bonn, Germany*

<sup>3</sup>*Université Paris-Saclay, CNRS, LPTMS, 91405, Orsay, France*

<sup>4</sup>*INFN, Sezione di Lecce, 73100 Lecce, Italy*

<sup>5</sup>*Department of Mathematics, Physics and Electrical Engineering, Northumbria University, Newcastle upon Tyne NE1 8ST, United Kingdom*

<sup>6</sup>*Institut Universitaire de France (IUF)*

## METHODS

The experiment conducted utilized a planar  $\text{Al}_x\text{Ga}_{1-x}\text{As}$  microcavity containing 12 GaAs quantum wells, with aluminium fractions of 0.2 and 0.95 in the distributed Bragg reflectors, kept at a temperature of approximately 5 K. A ring potential, with a radius of  $\sim 75$   $\mu\text{m}$ , is generated using an off-resonance CW laser beam ( $\lambda = 735$  nm), shaped by a spatial light modulator displaying a Bessel function. This potential confines the polariton fluid by inducing a local energy blueshift in the polariton resonance due to the high exciton density under the CW pump. To inject the polariton fluid into the center of this potential, a pulsed laser (pulse duration of 2 ps) is focused into a Gaussian spot with a beam waist of approximately 17  $\mu\text{m}$ . The excitation energy is slightly blue-detuned from the ground state by 1.2 meV (0.21 meV for the “low-energy” case reported in a later section), providing the polaritons with an initial kinetic energy that allows for their rapid expansion within the potential and subsequent hydrodynamic vortex formation upon collision with the potential barrier.

The time evolution of the polariton fluid is captured using off-axis digital holography, which involves the interference of the signal with a reference pulse (a sample of the excitation beam) with a variable time delay, enabling the retrieval of both the amplitude and phase of the fluid, as illustrated in Fig. S1. The temporal resolution is of around 1 ps and the spatial resolution is finer than the estimated healing length of the vortices. Each time frame is obtained by integrating over a large number of pulses, given the pulsed pump’s repetition rate of 80 MHz and the typical integration time of 1 ms. Despite the averaging, spatial inhomogeneities allows for the observation of coherent vortex dynamics. To ensure statistical significance, the analysis averaged four measurements by translating the sample in-plane to eliminate morphological effects. Different spatial configurations can be observed at different sample locations, yet the statistical properties of the observables remain consistent. For each experimental condition and time frame, we identify vortices and critical points by computing the circulation around each point of the two-dimensional phase map and the

corresponding velocity field, respectively, and searching for integer multiples of  $2\pi$ . From a simple comparison, we can further distinguish which of the critical points are nodes.

## BIFURCATION DETECTION

We give here a couple of examples of bifurcations such as those discussed in the main text, and detected during the time evolution of the experiment. The first is an instance where two nodes transform into a vortex-antivortex pair according to the mechanism in Eq. (2a) of the main text, which we recall here for completeness:

$$\text{node} + \text{node} \xrightarrow{\frac{a}{b}} \text{vortex}_{(+)} + \text{vortex}_{(-)}. \quad (\text{S1})$$

In the left panel of Fig. S2, we present two consecutive time frames of the same spatial region, highlighting the evolution of the flow pattern from a configuration containing nodes and saddles (at  $t = 15$  ps) to one where two nodes are transformed into a vortex and an antivortex ( $t = 16$  ps).

In the right panel of Fig. S2, the Bristol annihilation mechanism [Eq. (5) of the main text, reproduced here]

$$\text{vortex}_{(+)} + \text{vortex}_{(-)} + \text{saddle} + \text{saddle} \xrightarrow{\frac{e}{f}} \emptyset, \quad (\text{S2})$$

is observed in our experiment during the second stage of the dynamics, when dissipation begins to dominate ( $t > t_c = 56$  ps). Two consecutive frames (at times  $t = 76$  and  $t = 77$  ps) illustrate the simultaneous annihilation of two saddles and a vortex-antivortex pair within a laminar plane flow, marking the dissipation of incompressible kinetic energy from the system.

## VORTEX CLUSTERING

In the main text, we discussed the crossover time  $t_c$  at which the number of vortices, initially increasing significantly in the turbulent regime, starts a rapid decay. This time is non universal and depends on the initial configuration of the system. However, the survey of different

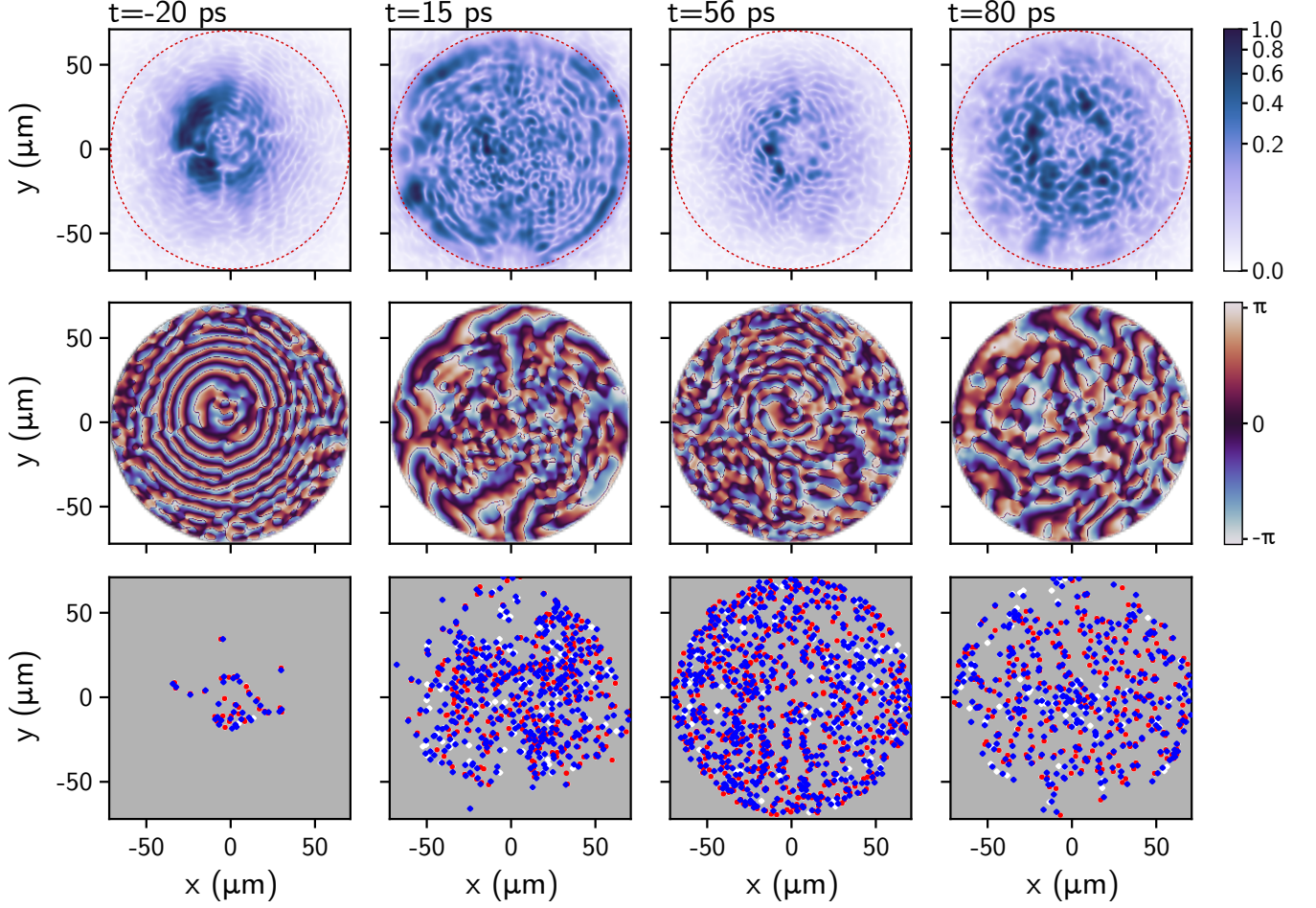


FIG. S1. Measured density (top), phase (middle), and critical points (bottom) of the polariton fluid for the high-energy case. At each time frame, the density is normalized to ensure its maximum value is 1. The dashed red circle represents the position of the confining potential. In the bottom row the white diamonds are nodes, the blue ones are saddles, and the red points are vortices (their signs are omitted for legibility). The time frames, from left to right, correspond to: the initial experimental condition ( $t = -20$  ps), when the polariton fluid is still mostly localized in the center of the potential and has yet to fill all the available space;  $t = 15$  ps after the sudden growth in the number of vortices, when the polariton fluid is flowing back after hitting the boundaries; the switching point at around  $t = 56$  ps, when vortex growth stops and the Bristol mechanism becomes relevant; and finally, a snapshot near the end of the dynamics at  $t = 80$  ps.

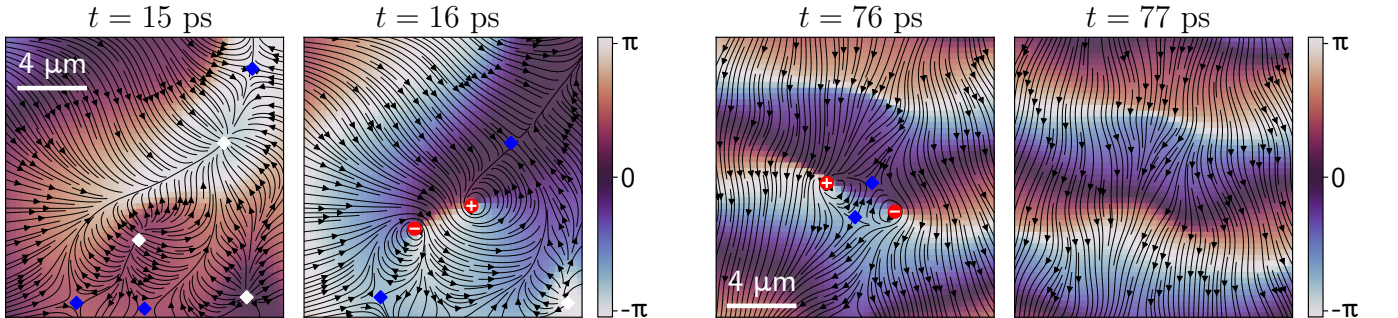


FIG. S2. (left) Experimental snapshots, taken at times  $t = 15$  and  $t = 16$  ps, showing the formation of a vortex-antivortex pair starting from two nearby nodes, as indicated by Eq. (S1). The streamlines of the velocity field  $\vec{v} = (\hbar/m)\vec{\nabla}\Theta$  are plotted as oriented solid lines, on top of the color-coded phase field  $\Theta(x, y)$ . (right) Experimental snapshots of streamlines and the phase field taken during stage 2 of the experiment, at times  $t = 76$  and  $t = 77$  ps, showing the annihilation of two saddles and a vortex-antivortex pair via the Bristol mechanism (S2).

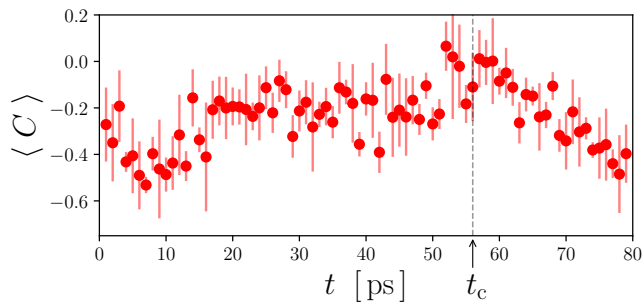


FIG. S3. Experimental correlation function (S3) averaged over 4 realizations plotted as a function of time. The dots correspond to the mean value, the vertical segments are the standard deviations. Adapted from Ref. [3].

observables characterizing the non-linear dynamics in the turbulent superfluid discussed in the main text indicates that  $t_c$  is also the time at which the inverse cascade stops and turbulence starts its decay.

A first simple remark is in order: if vortices of the same vorticity are gathered in packs they cannot annihilate since they need to encounter vortices of opposite vorticity to do so. Hence, clustering tends to prevent vortices from annihilating each other. An initial increase followed by a (faster) decrease of clustering is revealed in Fig. S3 which displays the average of the correlation function  $C$ , defined as [1, 2]

$$C = \frac{1}{V} \sum_{i=1}^V c_i, \quad (\text{S3})$$

where  $V$  is the total number of vortices and  $c_i = 1$  ( $-1$ ) if the vortex closest to a given vortex  $i$  has the same (opposite) vorticity. The largest possible value of the correlation function is  $C = +1$  and is reached for perfect clustering.  $C = -1$  is associated with the state of lowest energy and (positive) temperature; increasing values of  $C$  correspond to higher energetic states of the vortex gas. The figure shows that clustering starts to decrease at the same time  $t_c = 56$  ps at which vortex decay sets in. The concomitant decrease of clustering and of the number of vortices is an interesting test of coherence of the point of view we have on the phenomenology of the system, but is not in itself an explanation of the underlying physical mechanism. The results discussed in the main text suggest that it is the incompressible component of the kinetic energy which triggers both phenomena.

### LOW-ENERGY DATA SET

The data presented in the main text correspond to a turbulent regime in which a high-energy polariton superfluid is injected against a potential barrier. We consider

in this section a data set obtained at relatively low injection energy:  $E = E^{\text{low}} = 0.21$  meV here, instead of  $E^{\text{high}} = 1.20$  meV in the main text (both sets of data are extracted from the experiment of Ref. [3]).

The low-energy experimental results for the number of critical points, presented in Fig. S4, display a tendency to saturate: from  $t = 60$  ps on,  $V(t)$ ,  $S(t)$ , and  $N(t)$  vary quite slowly. To emulate this behavior, the dimensionless dynamical system for  $V$ ,  $S$  and  $N$  should have a fixed point. We recall the corresponding equations here for completeness [Eqs. (4) of the main paper]:

$$\begin{aligned} \frac{dv}{d\tau} &= n^2 - \alpha v^2, & \frac{ds}{d\tau} &= 1 - \gamma ns, \\ \frac{dn}{d\tau} &= 1 - n^2 - \gamma ns + \alpha v^2, \end{aligned} \quad (\text{S4})$$

where  $v = V/N_0$ ,  $S = S/N_0$ ,  $n = N/N_0$ ,  $\tau = t/t_0$  and  $\alpha$  and  $\gamma$  are re-scaled reaction rates.

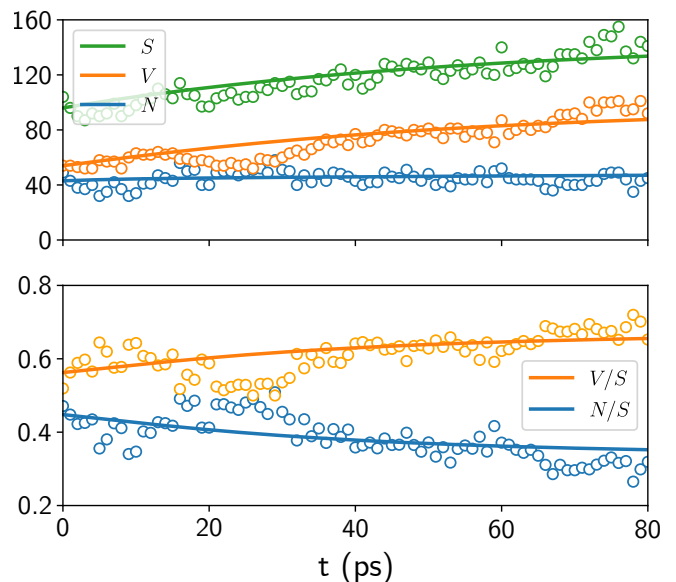


FIG. S4. Comparison of the experimental results of the low-energy data set for the numbers  $N(t)$  of nodes,  $V(t)$  of vortices, and  $S(t)$  of saddles (circles) with the numerical integration of Eqs. (S4) (solid lines).

The parameter  $\alpha$  needs to be finite for the system (S4) to have a fixed point. In this case, if we denote as  $n_\infty, v_\infty, s_\infty$  the coordinates of the fixed point, defining  $\beta = 1/\sqrt{\alpha}$  we get  $v_\infty = \beta n_\infty$ ,  $s_\infty = 1/(\gamma n_\infty)$  and

$$n_\infty = \frac{I_{P0} + \sqrt{I_{P0}^2 + 4(1 + \beta)/\gamma}}{2(1 + \beta)}. \quad (\text{S5})$$

In this expression  $I_{P0} = n + v - s$  is the constant value of the rescaled Poincaré index of the whole system ( $I_{P0} = I_P/N_0$ ). In the limit  $I_{P0}^2 \ll 4(1 + \beta)/\gamma$  [4], formula (S5) reads  $n_\infty = [\gamma(1 + \beta)]^{-1/2}$  and implies that  $s_\infty = (1 + \beta)n_\infty$ . Comparing the values  $v_\infty/n_\infty = \beta$  and  $s_\infty/n_\infty =$

$1+\beta$  with the experimental values  $V/N \approx 2$  and  $S/N \approx 3$  around  $t = 60$  ps points to a value  $\beta \approx 2$ , *i.e.*,  $\alpha = 0.25$ . We found that the choice  $\gamma = 1$ ,  $N_0 = 80$ ,  $t_0 = 27$  ps, and  $\alpha = 0.25$  gives a good account of the data set, see Fig. S4.

The system is not here in a turbulent regime such as the one studied in the main text. It is interesting to note that the value  $\alpha = 0.25$  corresponds to equality  $a = b$  in the node to vortex conversion (S1). Of course we can not ascertain exact equality, but it is clear that  $a \simeq b$  which implies that in the non-turbulent setting considered in the present section, the node-to-vortex conversion (S1) is on average in equilibrium. Remarkably, the situation is completely different in the turbulent setting considered in the main text, where  $b = 0$  which corresponds to a unidirectional reaction, increasing the number of vortices, as expected in the inverse cascade which occurs during the growth of turbulence.

Also, in the case considered in this section the injection energy  $E$  is smaller than in the turbulent case, the number of vortices increases at a lower pace, and the stage of decay (stage 2 in Fig. 3 of the main text) is not reached within the experimental time window. This interpretation of the different behaviors of the two data sets is corroborated by the following evalua-

tion of orders of magnitude: A simple dimensional argument suggests that the characteristic time  $t_0$  should scale as  $t_0 \propto E^{-1/2}$ . And indeed the characteristic times  $t_0^{\text{low}}$  and  $t_0^{\text{high}}$  for the two sets of data are in a ratio  $t_0^{\text{low}}/t_0^{\text{high}} = 27 \text{ ps}/11 \text{ ps} = 2.45$  which is consistent with the value  $\sqrt{E^{\text{high}}/E^{\text{low}}} = \sqrt{1.20 \text{ meV}/0.21 \text{ meV}} = 2.39$ .

- 
- [1] A. C. White, C. F. Barenghi, and N. P. Proukakis, Creation and characterization of vortex clusters in atomic Bose-Einstein condensates, *Phys. Rev. A* **86**, 013635 (2012).
  - [2] S. P. Johnstone, A. J. Groszek, P. T. Starkey, C. J. Billington, T. P. Simula, and K. Helmerson, Evolution of large-scale flow from turbulence in a two-dimensional superfluid, *Science* **364**, 1267 (2019).
  - [3] R. Panico, P. Comaron, M. Matuszewski, A. S. Lanotte, D. Trypogeorgos, G. Gigli, M. De Giorgi, V. Ardizzone, D. Sanvitto, and D. Ballarini, Onset of vortex clustering and inverse energy cascade in dissipative quantum fluids, *Nat. Photonics* **17**, 451 (2023).
  - [4] It can be checked *a posteriori* that this approximation is legitimate: the total experimental Poincaré index is  $I_P = \pm 2$  whereas  $N_0$  is of order  $10^2$ :  $I_{P_0}^2 \approx 10^{-4}$ . The term  $4(1 + \beta)/\gamma$  is instead of order unity.